

Article

Transient and Steady-State Performance Improvement of IM Drives Based on Dual-Torque Model

Xinyu Chen and Pingping Gong *

School of Electrical Engineering, Guangxi University, Nanning 530004, China; 2012301003@st.gxu.edu.cn

* Correspondence: gongpp@gxu.edu.cn

Abstract: Transient response performance and steady-state operation performance are the two most important performance indicators of a motor drive system. In order to solve these two problems, this study proposes a new induction motor (IM) model, and then designs a new simplified linearization controller method. First, the tangential force that determines the transient process of the motor is represented by electromagnetic torque, and the radial force is represented by reactive torque. Then, the dual-torque model of IM is derived, which not only accurately shows the rotating air-gap magnetic field through the amplitude and rotating angular frequency, but also visually demonstrates the physical essence of the transient process of IM. Then, this study proposes a simplified feedback linearization method without the analysis of zero dynamic. In addition, a time-scale hierarchical control system is designed to reduce the ripple caused by the coupling of different time-scale variables. The experimental results show that the steady-state torque ripple of the proposed method is 65% lower than that of RFOC, and the torque response speed is 10% higher than that of DTC.

Keywords: induction motor; dual-torque model; feedback linearization; time-scale; torque ripple; torque response



Citation: Chen, X.; Gong, P. Transient and Steady-State Performance Improvement of IM Drives Based on Dual-Torque Model. *Machines* **2023**, *11*, 490. <https://doi.org/10.3390/machines11040490>

Academic Editor: Ramani Kannan

Received: 13 March 2023

Revised: 14 April 2023

Accepted: 17 April 2023

Published: 19 April 2023



Copyright: © 2023 by the authors. Licensee MDPI, Basel, Switzerland. This article is an open access article distributed under the terms and conditions of the Creative Commons Attribution (CC BY) license (<https://creativecommons.org/licenses/by/4.0/>).

1. Introduction

In recent years, battery electric vehicles (BEVs) and plug-in hybrid electric vehicle (PHEVs) have been introduced as new energy vehicles that are driven by electric motors, and they have grown in popularity [1]. The performance of the induction motor (IM) drive system directly determines the motion performance of the vehicle. Fast response speed during acceleration and smooth operation while cruising are required by the IM drive system [2]. In other words, fast transient response speed and small steady state torque ripple are the critical issues of IM drives [3,4]; this involves two concepts: (a) the model; and (b) linearization.

Rotor field-oriented control (RFOC) and direct torque control (DTC) based on a two-phase perpendicular coordinate system are the two classical control algorithms for IMs. With rotating coordinate transformation, RFOC decompose the stator current into flux linkage current and torque current in $d - q$ axis to realize the linear control of torque and flux linkage [5]. This method shows high control accuracy but slow torque response speed. The decoupling relationship can only be established when the magnetic linkage amplitude has minimal fluctuations. Therefore, the RFOC is approximately decoupled. Rated excitation is not required under light load conditions, which leads to performance degradation [6]. When the electric vehicle accelerates and decelerates frequently, the fluctuation in the DC bus voltage also destabilizes the flux linkage, which then also weakens the control performance [7]. When the speed rises above the rated speed, the coupling between torque current and excitation current can become so large that it becomes out of control [8]. In the $\alpha - \beta$ axis, DTC selects the best voltage vector through the switch vector table to directly control the stator flux amplitude and electromagnetic torque. Therefore DTC shows faster torque response speed than RFOC. However, DTC has large torque and flux ripples,

and the switching frequency is not fixed, due to the hysteresis controller. To solve these problems, many methods have been proposed: SVM [9], constant switching frequency [10], the duty-cycle method [11], deadbeat control method [12], and neural network method [13]. These methods have reduced ripples with additional control parts, but often complicate the control structure. Both RFOC and DTC are based on quasi-transient state models instead of complete transient models, which makes the decoupling conditions essential. Therefore, in this case, it is impossible to improve both the transient and steady-state responses.

From the perspective of the physical mechanism, the essence of the flux linkage and torque changes during the transient is the change of reactive and active energies. Therefore, a thorough motor transient model was needed to describe this process. It is easy to use instantaneous active and reactive power to build a motor model. Indirect instantaneous reactive power and instantaneous active power (IPQC) directly use dual instantaneous power to control the rotating magnetic field to reduce the torque and flux ripples, but they include an additional current decoupling part [14]. A dual instantaneous power algorithm can also be directly applied to the motor drive without a current PI controller, resulting in increased current harmonics [15]. Furthermore, instantaneous reactive power and instantaneous active power directly determine the amplitude change rate and the rotation change rate of the stator magnetic field. The amplitude and angular frequency of the magnetic field have been used to establish the transient model of the motor. A model obtained from a large amount of test data could describe the process from power supply voltage and frequency to amplitude and phase of response [16]. However, this conclusion has yet to be experimentally proven.

The next problem is the linearization of torque and flux linkage. In contrast to the traditional local linearization using Taylor series expansion near the stable operation point, the global linearization method does not ignore any higher-order nonlinear term in the linearization process, so this method is accurate [17,18]. Input-output linearization is a classical global linearization method that can decouple the motor system into the independent flux linkage system and torque system. By deducing the affine nonlinear model and selecting the differential homeomorphism transformation, the decoupling controller is designed through the state feedback control law [19–21]. When the relative-degree of the system is not equal to the order of the system, the complex zero dynamic problem must be discussed before the decoupling controller can be designed [22]. The input-output linearization steps are numerous and have no clear physical definitions, which has limited its applications. In order to simplify these methods, a direct feedback linearization control (DFL) based on input-output linearization was proposed; this could also realize the decoupling of torque and flux linkage [23].

Therefore, an accurate description of the motor transient and global linearization are two key issues to consider for high-performance motor control algorithms. Reference [24] selected the scalar product and the vector product of the stator and rotor flux vectors, as well as the square signal of the flux amplitude, to construct the mathematical model of an IM and proposed a sliding-mode variable control structure based on feedback linearization, which improves the robustness and steady-state control accuracy of the system. This method could accurately describe the transient process of the motor and achieve global decoupling. However, this method still had some shortcomings: (1) it did not explain the physical significance of the new variables and models; and (2) sliding mode transformation achieved good results but complicated the algorithm.

This paper proposes a new IM model and a new control algorithm, which could effectively reduce the steady-state ripple and improve the transient torque response speed. First, the tangential action of the rotating magnetic field of IM is characterized by the reactive torque, and then the mathematical model with the reactive torque and the electromagnetic torque as state variables could be expressed as a dual-torque model. This model directly shows the changes in reactive and active energy in the transient process of IM, which is the physical quantity essence of the motor transient. The electromagnetic torque and reactive torque are naturally perpendicular in space, which could greatly simplify the analysis

process of feedback linearization and avoid the zero-dynamic problem. In addition, the dual-torque control system is linearized into two cascaded first-order systems, so its stability is easy to explain. Then, we designed a control method based on different time scales to reduce the pulsation caused by the stator flux and the torque coupling, which is the defect of DTC. Finally, the electromagnetic torque and reactive torque are directly applied as the inner-loop feedback to speed up the torque response speed, and this improves the defects of RFOC. The proposed method is verified on an experimental platform of IM driven by a two-level inverter controlled by a dSPACE DS1104 controller.

2. Conventional Model of IM Drives

2.1. Mathematical Model of IM

In the rotating two-phase perpendicular coordinate system, the state space equations of squirrel-cage IM are as follows:

$$\frac{di_{sd}}{dt} = \frac{L_m R_r}{\sigma L_s L_r^2} \psi_{rd} + \frac{L_m}{\sigma L_s L_r} \omega \psi_{rq} - \frac{R_s L_r^2 + R_r L_m^2}{\sigma L_s L_r^2} i_{sd} + \omega_1 i_{sq} + \frac{1}{\sigma L_s} u_{sd} \quad (1)$$

$$\frac{di_{sq}}{dt} = \frac{L_m R_r}{\sigma L_s L_r^2} \psi_{rq} - \frac{L_m}{\sigma L_s L_r} \omega \psi_{rd} - \frac{R_s L_r^2 + R_r L_m^2}{\sigma L_s L_r^2} i_{sq} - \omega_1 i_{sd} + \frac{1}{\sigma L_s} u_{sq} \quad (2)$$

$$\frac{d\psi_{rd}}{dt} = -\frac{R_r}{L_r} \psi_{rd} + (\omega_1 - \omega) \psi_{rq} + \frac{L_m R_r}{L_r} i_{sd} \quad (3)$$

$$\frac{d\psi_{rq}}{dt} = -\frac{R_r}{L_r} \psi_{rq} - (\omega_1 - \omega) \psi_{rd} + \frac{L_m R_r}{L_r} i_{sq} \quad (4)$$

$$T_e = J \frac{1}{n_p} \frac{d\omega}{dt} + T_L \quad (5)$$

where: u is winding voltage; R is winding resistance; i is winding current; ψ is flux linkage; ω is rotor speed; and L is winding inductance. s and r represent the stator components and rotor components respectively; L_m is the mutual inductance between stator winding and rotor winding; T_e is electromagnetic torque, or active torque; T_L is load torque; J is rotary inertia; n_p is pole pairs of motor; ω_1 is angular frequency of stator magnetic field; and the d and q represent d -axis and q -axis components respectively. σ is leakage inductance, and $\sigma = 1 - (L_m^2 / L_s L_r)$.

The electromagnetic torque T_e can be expressed by the following:

$$T_e = \frac{3 n_p L_m}{2 L_r} (i_{sq} \psi_{rd} - i_{sd} \psi_{rq}) \quad (6)$$

In the stationary two-phase perpendicular coordinate system, the state-space equations of squirrel-cage IM are expressed as follows:

$$\frac{di_{s\alpha}}{dt} = \frac{R_r}{\sigma L_s L_r} \psi_{s\alpha} + \frac{1}{\sigma L_s} \omega \psi_{s\beta} - \left(\frac{R_s}{\sigma L_s} + \frac{R_r}{\sigma L_r} \right) i_{s\alpha} - \omega i_{s\alpha} + \frac{1}{\sigma L_s} u_{s\alpha} \quad (7)$$

$$\frac{di_{s\beta}}{dt} = \frac{R_r}{\sigma L_s L_r} \psi_{s\beta} - \frac{1}{\sigma L_s} \omega \psi_{s\alpha} - \left(\frac{R_s}{\sigma L_s} + \frac{R_r}{\sigma L_r} \right) i_{s\beta} + \omega i_{s\alpha} + \frac{1}{\sigma L_s} u_{s\beta} \quad (8)$$

$$\frac{d\psi_{s\alpha}}{dt} = u_{s\alpha} - R_s i_{s\alpha} \quad (9)$$

$$\frac{d\psi_{s\beta}}{dt} = u_{s\beta} - R_s i_{s\beta} \quad (10)$$

$$T_e = J \frac{1}{n_p} \frac{d\omega}{dt} + T_L \quad (11)$$

The electromagnetic torque T_e can be rewritten as follows:

$$T_e = \frac{3}{2} n_p (\psi_{s\alpha} i_{s\beta} - \psi_{s\beta} i_{s\alpha}) \quad (12)$$

where, α and β represent α -axis and β -axis components, respectively.

2.2. Conventional RFOC

The basic principle of RFOC is to control the torque and flux linkage through the decoupled excitation current i_{sd} and torque current i_{sq} , respectively, by coordinate revolution transformation according to the rotor field orientation.

When the direction of the rotor magnetic field is aligned with the d-axis of the rotor rotating magnetic field,

$$\psi_{rd} = \psi_r \quad (13)$$

$$\psi_{rq} = 0 \quad (14)$$

The necessary conditions for RFOC is $\frac{d\psi_r}{dt} \approx 0$, and then by substituting (19) and (20) into (7)–(12), we obtain

$$\psi_r = L_m i_{sd} \quad (15)$$

$$T_e = \frac{3}{2} n_p \frac{L_m^2}{L_r} i_{sq} \quad (16)$$

From the previous two equations, we know that ψ_r can be adjusted by i_{sd} and T_e can be adjusted by i_{sq} . These two processes are independent of each other.

2.3. Conventional DTC–SVM

The basic principle of DTC–SVM is to control the electromagnetic torque and stator flux linkage simultaneously by adjusting the stator voltage vector.

Since the stator resistance voltage drop is so small, R_s can be ignored. Formula (1) can be rewritten as follows:

$$u_s = \frac{d\psi_s}{dt} \quad (17)$$

The above equation can be approximately rewritten as follows:

$$\Delta \vec{\psi}_s = \vec{u}_s \Delta t \quad (18)$$

The electromagnetic torque T_e can be written as follows:

$$T_e = \frac{3}{2} n_p \frac{L_m}{\sigma L_s L_r} \psi_s \psi_r \sin \rho_{sr} \quad (19)$$

where, t is time, ρ_{sr} represents phase angle between ψ_s and ψ_r .

In order to accurately control the electromagnetic torque, it is necessary to keep the amplitude of ψ_s constant and keep the trajectory of its track circular. This is achieved through the hysteresis comparison controller in the initial DTC, which lead to increments in ripples of torque and flux. To maintain minimal ripples, space vector modulation (SVM) is introduced into the control system.

3. The Proposed Method

The core of the electromechanical energy conversion of IM is a rotating air-gap magnetic field. As a rotating object, its dynamic characteristics can be better described by the

amplitude and the rotational angular frequency, as compared to the Cartesian coordinate system. When the IM is disturbed, its torque and flux linkage change. As compared to its steady-state operation, this is directly reflected by the change of the amplitude and angular frequency of the rotating magnetic field. Essentially, this is the change of the instantaneous reactive power and instantaneous active power from the perspective of power balance.

The rotating air-gap magnetic field induces the stator rotating voltage vector in the stator winding and the rotor rotating voltage vector in the rotor winding. The rotor rotating voltage vector is directly related to the output torque. Because the stator leakage inductance of the IM is relatively small as compared to the mutual inductance, the stator resistance is also small, and the rotor electromotive force amplitude of the IM is approximately equal to the stator side voltage amplitude. Moreover, the rotor electromotive force rotation frequency is the same as the synchronous rotation frequency.

3.1. Dual-Torque Model of IM

The model shown by Formulas (7)–(11) is the most widely applied IM model, which is based on the mathematical relationship between various state variables. However, due to the high-order, nonlinear, and coupling characteristics of IM, the model cannot directly represent the physical essence of the transient process of IM.

Based on the dynamics of motor rotating voltage vector, IPQC establishes a model reflecting the transient process of the motor using instantaneous reactive power and instantaneous active power. However, the power quantity is not a dynamic variable, so the model cannot directly describe the dynamics of IM transient process. Therefore, we attempted to characterize the flux linkage with the reactive torque, and then we deduced the dynamic characteristics of the motor transient with the reactive torque and electromagnetic torque.

According to the description of the instantaneous power on the amplitude and the rotation angle frequency of the stator rotating voltage vector, the reactive torque should be the radial force, which determines its amplitude movement. The electromagnetic torque should be the tangential force, which determines its rotation angle frequency movement. Moreover, the reactive torque must be an electrical quantity in the same category as electromagnetic torque. Therefore, reactive torque is the duality of electromagnetic torque in both physics and mathematics. The equivalent physical model of IM is shown in Figure 1.

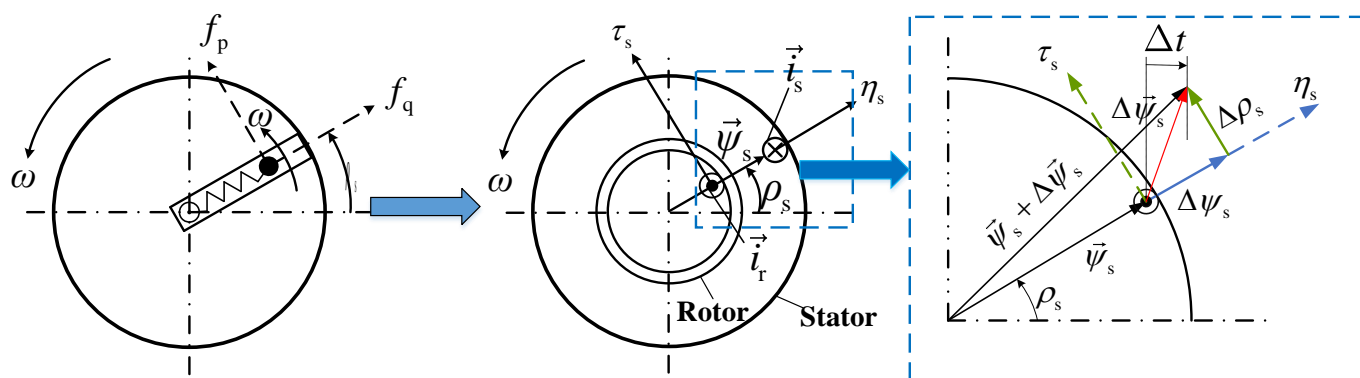


Figure 1. Schematic diagram of IM motion process.

The normalized electromagnetic torque is defined as the vector product of the stator flux linkage vector and the stator current, as follows:

$$\tau_s = \psi_s \otimes i_s \tag{20}$$

The normalized reactive torque is the duality of the electromagnetic torque, so it should be expressed by the scalar product of the stator flux linkage vector and the stator current vector as follows:

$$\eta_s = \psi_s \odot i_s \tag{21}$$

where τ_s represents the normalized electromagnetic torque, η_s represents the normalized reactive torque, \otimes represents vector product, and \odot represents scalar product.

Next, the appropriate state variables should be selected. Evidently,

$$\tau_s = \psi_{s\alpha} i_{s\beta} - \psi_{s\beta} i_{s\alpha} \tag{22}$$

$$\eta_s = \psi_{s\alpha} i_{s\alpha} + \psi_{s\beta} i_{s\beta} \tag{23}$$

Considering the rotating magnetic field, the other two state variables are the amplitude and phase of the stator rotating magnetic field, as follows:

$$\psi_s^2 = \psi_{s\alpha}^2 + \psi_{s\beta}^2 \tag{24}$$

$$\rho = \arctan\left(\frac{\psi_{s\beta}}{\psi_{s\alpha}}\right) \tag{25}$$

$$\omega = \dot{\rho} \tag{26}$$

After calculating the differential of Formulas (22)–(25), we substituted Formulas (7)–(11) into the result. The dual-torque model can be written as follows:

$$\begin{aligned} \frac{d\tau_s}{dt} = & -\frac{R_s L_r + R_r L_s}{\sigma L_s L_r} \tau_s + \left(-\frac{\psi_{s\beta}}{\sigma L_s} + \frac{\eta_s \psi_{s\beta}}{\psi_s^2} + \frac{\tau_s \psi_{s\alpha}}{\psi_s^2}\right) u_{s\alpha} + \left(\frac{\psi_{s\alpha}}{\sigma L_s} - \frac{\eta_s \psi_{s\alpha}}{\psi_s^2} + \frac{\tau_s \psi_{s\beta}}{\psi_s^2}\right) u_{s\beta} \\ & + \omega \eta_s - \frac{1}{\sigma L_s} \omega \psi_s^2 \end{aligned} \tag{27}$$

$$\begin{aligned} \frac{d\eta_s}{dt} = & -\frac{R_s L_r + R_r L_s}{\sigma L_s L_r} \eta_s + \left(\frac{\psi_{s\alpha}}{\sigma L_s} - \frac{\tau_s \psi_{s\beta}}{\psi_s^2} + \frac{\eta_s \psi_{s\alpha}}{\psi_s^2}\right) u_{s\alpha} + \left(\frac{\psi_{s\beta}}{\sigma L_s} + \frac{\tau_s \psi_{s\alpha}}{\psi_s^2} + \frac{\eta_s \psi_{s\beta}}{\psi_s^2}\right) u_{s\beta} \\ & - \omega \tau_s + \frac{R_r}{\sigma L_s L_r} \psi_s^2 - R_s \frac{\tau_s^2 + \eta_s^2}{\psi_s^2} \end{aligned} \tag{28}$$

$$\frac{d\rho_s}{dt} = -R_s \frac{\tau_s}{\psi_s^2} + \frac{\psi_{s\alpha}}{\psi_s^2} u_{s\beta} - \frac{\psi_{s\beta}}{\psi_s^2} u_{s\alpha} \tag{29}$$

$$\frac{d\psi_s^2}{dt} = -2R_s \eta_s + \psi_{s\alpha} u_{s\alpha} + \psi_{s\beta} u_{s\beta} \tag{30}$$

In consideration of rotor speed dynamics, Formula (17) can be rewritten as the following:

$$\frac{d\omega}{dt} = \frac{n_p}{J} \left(\frac{3}{2} n_p \tau_s - T_L\right) \tag{31}$$

Formulas (29) and (31) indicate that the rotation angle frequency or the magnetic phase of the stator flux can also be selected as the output quantity. However, the phase is not the response when the dual torque acts directly on the rotating magnetic field. It is just the reflection of the frequency difference between the IM rotating magnetic field and the power voltage vector \vec{u}_s due to the disturbance. The phase angle ρ_s cannot directly reflect the dynamic changes of the induction motor at that moment. Then, the output variables of the dual-torque model should be selected as the amplitude of the stator flux and the rotation angle frequency. The dual-torque model is completely described by the Formulas (27), (28), (30), and (31). In other words, the dual torque model is a fourth-order model described by reactive torque η_s , electromagnetic torque τ_s , square of the amplitude of the stator flux linkage ψ_s^2 , and rotation angle frequency ω . The dual-torque model directly relates the input instantaneous power on the stator side and the torque on the rotor side dynamically.

3.2. Linearization of Dual-Torque Model

Although the dual-torque model intuitively represents the transient essence of IM, torque coupling in Formulas (27) and (28) still exists, and it is a coupled nonlinear system. It is necessary to decouple the dual torque. In order to ensure unconditional decoupling, the

local linearization near the steady working point is not feasible. Input-output linearization requires the construction of an affine nonlinear model with complex steps and no clear physical significance. According to Formulas (20) and (21), the dual-torque coordinate system can be expressed as shown in Figure 2. As shown in Figure 2, the dual-torque is naturally orthogonal in the space, which indicates that the decoupling controller based on the dual-torque model has strong decoupling performance, because this perpendicular is unconditional.

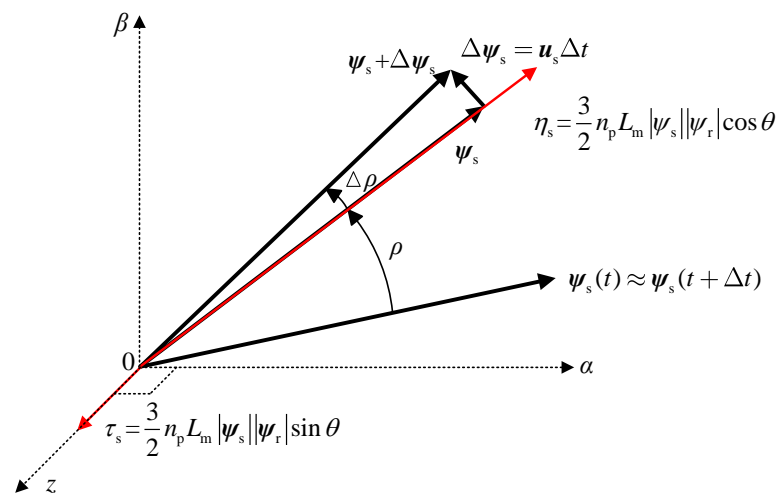


Figure 2. Schematic diagram of dual-torque coordinate system.

This method must also analyze the zero-dynamic stability problem. A simple state transformation method that can realize linearization is proposed. Based on the aforementioned dual-torque model, the proposed method simplified the conventional FBL.

Two variables can be defined by the following:

$$k_q = \left(-\frac{\psi_{s\beta}}{\sigma L_s} + \frac{\eta_s \psi_{s\beta}}{\psi_s^2} + \frac{\tau_s \psi_{s\alpha}}{\psi_s^2} \right) u_{s\alpha} + \left(\frac{\psi_{s\alpha}}{\sigma L_s} - \frac{\eta_s \psi_{s\alpha}}{\psi_s^2} + \frac{\tau_s \psi_{s\beta}}{\psi_s^2} \right) u_{s\beta} + \omega \eta_s - \frac{1}{\sigma L_s} \omega \psi_s^2 \tag{32}$$

$$k_d = \left(\frac{\psi_{s\alpha}}{\sigma L_s} - \frac{\tau_s \psi_{s\beta}}{\psi_s^2} + \frac{\eta_s \psi_{s\alpha}}{\psi_s^2} \right) u_{s\alpha} + \left(\frac{\psi_{s\beta}}{\sigma L_s} + \frac{\tau_s \psi_{s\alpha}}{\psi_s^2} + \frac{\eta_s \psi_{s\beta}}{\psi_s^2} \right) u_{s\beta} - \omega \tau_s + \frac{R_r}{\sigma L_s L_r} \psi_s^2 - R_s \frac{\tau_s^2 + \eta_s^2}{\psi_s^2} \tag{33}$$

These two variables can be used as the input signals for the dual-torque decoupling. Then, the nonlinear system can be written as the following linear system:

$$\frac{d\tau_s}{dt} = -\frac{R_s L_r + R_r L_s}{\sigma L_s L_r} \tau_s + k_q \tag{34}$$

$$\frac{d\eta_s}{dt} = -\frac{R_s L_r + R_r L_s}{\sigma L_s L_r} \eta_s + k_d \tag{35}$$

$$\frac{d\omega}{dt} = \frac{n_p}{J} \left(\frac{3}{2} n_p \tau_s - T_L \right) \tag{36}$$

$$\frac{d\psi_s^2}{dt} = -2R_s \eta_s + \psi_{s\alpha} u_{s\alpha} + \psi_{s\beta} u_{s\beta} \tag{37}$$

It is obvious that k_q and k_d control τ_s and η_s as input signals, respectively, and then τ_s and η_s control ω and ψ_s^2 , respectively.

The next step is to find a state transformation. We solved Formulas (32) and (33), as follows:

$$u_{s\alpha} = \frac{x_{22}}{y} (k_q - \omega\eta_s + \frac{1}{\sigma L_s} \omega\psi_s^2) - \frac{x_{12}}{y} (k_d + \omega\tau_s - \frac{R_r}{\sigma L_s L_r} \psi_s^2 + R_s \frac{\tau_s^2 + \eta_s^2}{\psi_s^2}). \tag{38}$$

$$u_{s\beta} = \frac{x_{11}}{y} (k_d + \omega\tau_s - \frac{R_r}{\sigma L_s L_r} \psi_s^2 + R_s \frac{\tau_s^2 + \eta_s^2}{\psi_s^2}) - \frac{x_{21}}{y} (k_q - \omega\eta_s + \frac{1}{\sigma L_s} \omega\psi_s^2) \tag{39}$$

where

$$\begin{aligned} x_{11} &= -\frac{\psi_{s\beta}}{\sigma L_s} + \frac{\eta_s \psi_{s\beta}}{\psi_s^2} + \frac{\tau_s \psi_{s\alpha}}{\psi_s^2} \\ x_{12} &= \frac{\psi_{s\alpha}}{\sigma L_s} - \frac{\eta_s \psi_{s\alpha}}{\psi_s^2} + \frac{\tau_s \psi_{s\beta}}{\psi_s^2} \\ x_{21} &= \frac{\psi_{s\alpha}}{\sigma L_s} - \frac{\tau_s \psi_{s\beta}}{\psi_s^2} + \frac{\eta_s \psi_{s\alpha}}{\psi_s^2} \\ x_{22} &= \frac{\psi_{s\beta}}{\sigma L_s} + \frac{\tau_s \psi_{s\alpha}}{\psi_s^2} + \frac{\eta_s \psi_{s\beta}}{\psi_s^2} \end{aligned} \tag{40}$$

$$y = x_{11}x_{22} - x_{12}x_{21} = \frac{\tau_s^2 + \eta_s^2}{\psi_s^2} - \frac{\psi_s^2}{(\sigma L_s)^2} \tag{41}$$

In order to ensure the feasibility of this linearization, it is necessary to ensure that the transformation matrix from the control signals k_q and k_d to the reference voltage $u_{s\alpha}$ and $u_{s\beta}$ is invertible, respectively. Based on Formulas (38) and (39), we know that the transformation matrix P can be written as follows:

$$P = \frac{1}{y} \begin{pmatrix} x_{11} & x_{12} \\ x_{21} & x_{22} \end{pmatrix} = \frac{(\sigma L_s)^2 \psi_s^2}{(\tau_s^2 + \eta_s^2)(\sigma L_s)^4 - \psi_s^4} \begin{pmatrix} x_{11} & x_{12} \\ x_{21} & x_{22} \end{pmatrix} \tag{42}$$

The magnetic leakage coefficient $\sigma \ll 1$, and it is consistently found that stator flux linkage ψ_s , the stator inductance L_s , the reactive torque η_s , and the electromagnetic torque τ_s are not zero when the motor was running, so the above formula is always reversible. In other words, this state transformation always exists, so the proposed feedback linearization is valid. Therefore, the proposed method can realize the global decoupling of ψ_s^2 and T_e . The system described in Formulas (40)–(43) can be easily divided into two subsystems, as follows:

$$\begin{aligned} \frac{d\tau_s}{dt} &= -\frac{R_s L_r + R_r L_s}{\sigma L_s L_r} \tau_s + k_q \\ \frac{d\omega}{dt} &= \frac{n_p}{J} (\frac{3}{2} n_p \tau_s - T_L) \end{aligned} \tag{43}$$

$$\begin{aligned} \frac{d\eta_s}{dt} &= -\frac{R_s L_r + R_r L_s}{\sigma L_s L_r} \eta_s + k_d \\ \frac{d\psi_s^2}{dt} &= -2R_s \eta_s + \psi_{s\alpha} u_{s\alpha} + \psi_{s\beta} u_{s\beta} \end{aligned} \tag{44}$$

Formula (49) represents the conversion process of electric energy to mechanical energy, and Formula (50) represents the conversion process of electric energy to magnetic energy. Furthermore, ω can be controlled by k_q , and ψ_s^2 can be controlled by k_d . These two processes are independent of each other, so ω and ψ_s^2 are decoupled.

3.3. Stability Analysis of Dual-Torque Controller

Reference [25] elaborated on the inevitable zero dynamic problem in feedback linearization. The main content of feedback linearization was to transform a nonlinear system into a linear system through a set of nonlinear coordinate transformations. According to the relationship between the system order n and the relative order r of the system, it could be discussed in two cases: (1) when $r = n$, the nonlinear system could be precisely linearized by nonlinear feedback; and (2) when $r < n$, there will inevitably be an $n - r$ order zero dynamic subsystem, which was unobservable. Therefore, if the zero dynamic subsystem was unstable, then the entire system cannot be asymptotically stable. Regardless of the method used for feedback linearization, this issue must be addressed.

The output equation of the system is expressed as follows:

$$y = \begin{pmatrix} y_1 \\ y_2 \end{pmatrix} = \begin{pmatrix} h_1(x) \\ h_2(x) \end{pmatrix} = \begin{pmatrix} \omega \\ \psi_s^2 \end{pmatrix} \quad (45)$$

For the subsystem described in Formula (43), the second derivative of ω appears as τ_s , so the relative-order of first subsystem is 2. For the subsystem described in Formula (44), the second derivative of ψ_s^2 appears as η_s , so the relative order of second subsystem is 2. Therefore, the relative order of the system is 4. According to Section 3.1, the dual-torque model is a fourth-order model. Therefore, the relative-order of the dual-torque model is equal to the system order. Based on the above theory, the proposed method will not exhibit zero dynamic subsystems. Therefore, as compared to conventional method [26], the proposed method avoids the occurrence of zero dynamic problems.

In addition, since the decoupled dual-torque model is linear, the classical linear system theory can be used to analyze its stability. Because the poles of the differential equations of τ_s and η_s are located in the left half-plane, the controller is stable. Consequently, the proposed linearization method is an effective and simplified method.

3.4. Multi-Time Scale Control System Based on Dual-Torque Model

After the nonlinear and coupled system model is converted into a linearized and decoupled system model, the linear control method can be applied. For the simple system described by Formulas (49) and (50), the closed-loop control system can be designed with PI controller, as follows:

$$\begin{aligned} k_q &= k_{11}(\eta_s^{\text{ref}} - \eta_s) + k_{12} \int_0^t (\eta_s^{\text{ref}}(x) - \eta_s(x)) dx \\ \eta_s^{\text{ref}} &= k_{13}(\omega_s^{\text{ref}} - \omega_s) + k_{14} \int_0^t (\omega_s^{\text{ref}}(x) - \omega_s(x)) dx \end{aligned} \quad (46)$$

$$\begin{aligned} k_d &= k_{21}(\tau_s^{\text{ref}} - \tau_s) + k_{22} \int_0^t (\tau_s^{\text{ref}}(x) - \tau_s(x)) dx \\ \eta_s^{\text{ref}} &= k_{23}(\psi_s^{2\text{ref}} - \psi_s^2) + k_{24} \int_0^t (\psi_s^{2\text{ref}}(x) - \psi_s^2(x)) dx \end{aligned} \quad (47)$$

The rotational speed is a mechanical quantity, so it is a slow variable with a change rate of 1000 ms, according to Table A1. The dynamic characteristics of the magnetic linkage are determined by the rotor time constant

$$\tau_r = \frac{L_r}{R_r} \quad (48)$$

By substituting the data from Table A2 into Formula (48), the time-variation scale is approximately 111 ms.

The time-variation scale of electromagnetic torque can be expressed by the following formula:

$$\tau_\eta = \frac{\sigma L_s}{R_s + \left(\frac{L_m}{L_r}\right)^2 R_r} \quad (49)$$

By substituting the data from Table A2 into Formula (49), the time-variation scale is approximately 3.06 ms. According to Formulas (22) and (23), reactive torque and electromagnetic torque are physical quantities in the same category, so they have the same time-variation scale.

In summary, the rotational speed ω and the flux linkage ψ_s are the state quantities of the same slow time scale, whereas the electromagnetic torque τ_s and the reactive torque η_s are fast variables. The conventional IM control system controls the flux and torque simultaneously, and the state variables of different time scales are coupled, resulting in torque and flux ripples.

The reactive torque and electromagnetic torque proposed in this paper are physical quantities in the same category that describe the same physical object, so they have the same time scale. The state variable is changed to dual torque, from torque and flux linkage.

The control system proposed in this paper places the dual-torque on the same layer of the inner loop and places the flux and speed control on the same layer of the outer loop, which reduces the torque ripple caused by the coupling of state variables at different time scales. The control system structure block diagram was created based on the aforementioned theoretical analysis, and it is shown in Figure 3.

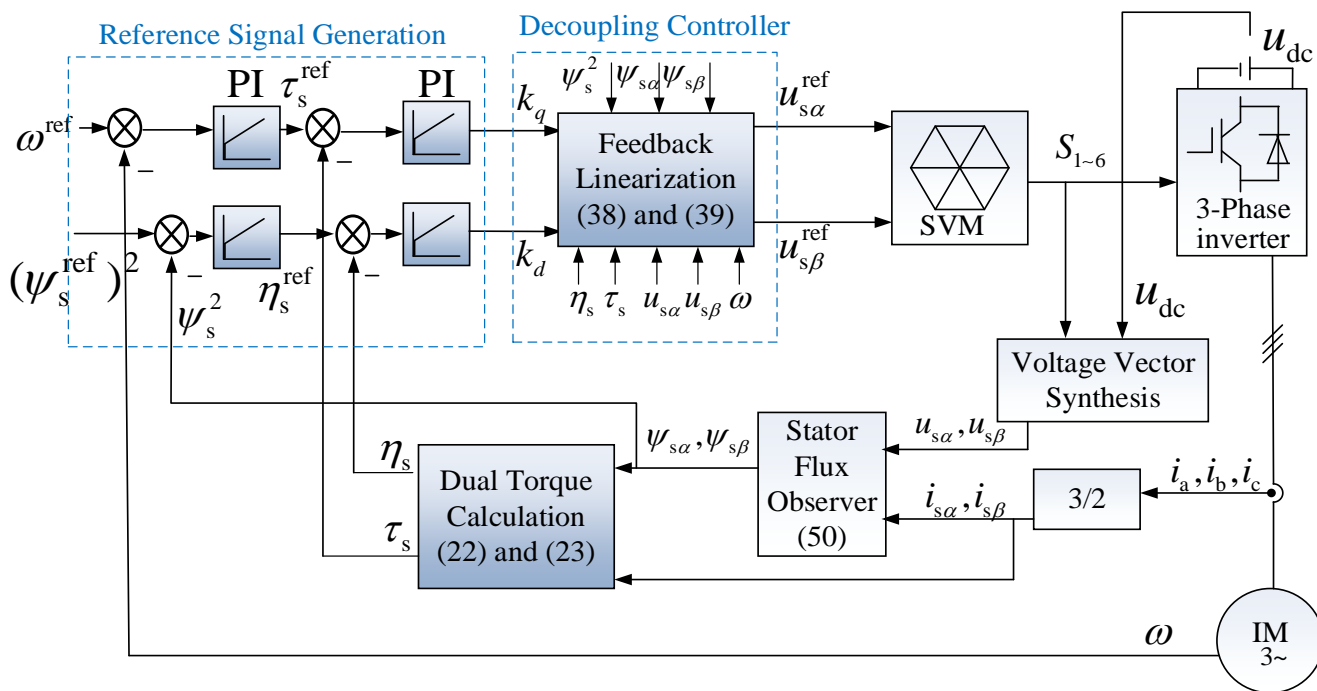


Figure 3. IM control system diagram with Proposed Method.

3.5. Dual-Torque Calculation and Stator Flux Observation

Reference Signal Generator: The error between the speed signal ω^{ref} of the external controller and the measured speed signal ω generates the electromagnetic torque command τ_s^{ref} through the PI controller; then, the error between the electromagnetic torque command τ_s^{ref} and the measured electromagnetic torque τ_s generates control signal k_q through the PI controller. The error between the magnetic linkage square command $(\psi_s^{ref})^2$ of the external controller and the measured magnetic linkage amplitude square $(\psi_s)^2$ generates the reactive torque command τ_s^{ref} through the PI controller. Finally, the error between the reactive torque command τ_s^{ref} and the measured reactive torque τ_s generates the control signal k_d through the PI controller.

Signal Measurement and Calculation: The rotor speed is directly measured by the speed sensor, and the three-phase current signal is measured by the current sensor of each phase. The stator voltage signal is directly synthesized from the DC bus voltage and the output signal of the inverter, which can reduce the noise signal in the direct measurement process. The calculation method of stator flux linkage ψ_s is as follows:

$$\begin{aligned} \psi_{s\alpha} &= \int (u_{s\alpha} - R_s i_{s\alpha}) dt \\ \psi_{s\beta} &= \int (u_{s\beta} - R_s i_{s\beta}) dt \end{aligned} \tag{50}$$

$$\psi_s^2 = \psi_{s\alpha}^2 + \psi_{s\beta}^2 \tag{51}$$

This analysis shows that the methods proposed in this study do not use a rotation coordinate transformation. Moreover, the dual-torque signals calculated by stator voltage ψ_s and stator current i_s are directly used as the inner-loop feedback signal, which improves the torque response speed.

Decoupled Controller: The controller parameters include the square of the flux amplitude ψ_s^2 ; the component of the flux amplitude $\psi_{s\alpha}$ and $\psi_{s\beta}$; the reactive torque η_s ; the electromagnetic torque τ_s ; the voltage component $u_{s\alpha}$ and $u_{s\beta}$; and the rotor speed ω . After control signals k_q and k_d are input to the controller, the controller will output signals $u_{s\alpha}$ and $u_{s\beta}$, respectively. Because the error between the actual value $u_{s\alpha}$, $u_{s\beta}$ and the command values $u_{s\alpha}^{\text{ref}}$, $u_{s\beta}^{\text{ref}}$ is very small, the command value of the control voltage can be regarded as the actual value, that is $u_{s\alpha}^{\text{ref}} = u_{s\alpha}$ and $u_{s\beta}^{\text{ref}} = u_{s\beta}$.

4. Results and Analysis of Experiment

In order to verify the proposed algorithm, the experiment was implemented based on the dSPACE DS1104 controller platform for IM drives. The sampling frequency was 10 kHz, and the DC bus voltage was 300 V. The rotor speed was measured by the speed encoder. The parameters of the IM used in the experiment are shown in Table A2.

The calculation formula for calculating the pulsation of the torque and the stator flux amplitude in steady state is as follows:

$$T_{\text{ripple}} = \sqrt{\frac{1}{N} \sum_{n=1}^N (T(n) - \bar{T})^2} \quad (52)$$

where, T_{ripple} is ripple of torque, $T(n)$ is value at the n-th point, \bar{T} is the average of the selected data, and N is number of sampling points.

The experimental group was the proposed method, and the control group was RFOC and DTC-SVM. In order to ensure the effectiveness of the experiment, the same speed PI parameters were used in the three experiments. The experimental equipment is shown in Figure 4.

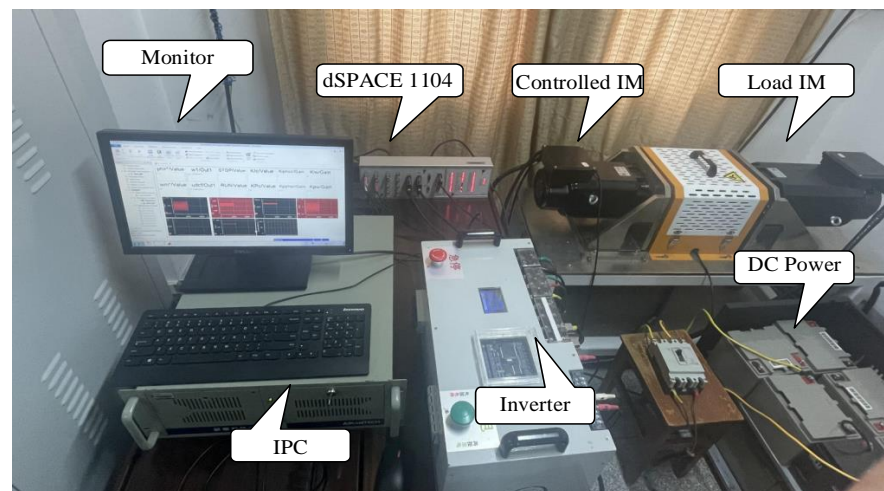


Figure 4. Pictures of the experimental platform.

4.1. Step Speed Transient Characteristic

Firstly, the speed characteristics of the proposed method were studied and compared with RFOC and DTC-SVM. The flux linkage amplitude was 0.5 Wb, and the motor was set at 100 rpm after starting; after this, a speed command of 500 r/min was given. The step speed response characteristics of the three methods are shown in Figure 5. The three methods could accurately track the reference speed, and the overshoot was zero. The experimental results showed that the speed response time of the proposed method was 8 ms faster than RFOC and 3 ms faster than DTC-SVM. In terms of torque, the torque variation of the three methods is very fast. The torque ripples of the proposed method were much smaller than that of DTC-SVM and RFOC. The proposed method had good

decoupling performance. In addition, the current harmonics of the proposed method were still smaller than RFOC, whereas those of DTC-SVM are obvious. Clearly, the flux ripple of the proposed method is smaller than that of DTC-SVM.

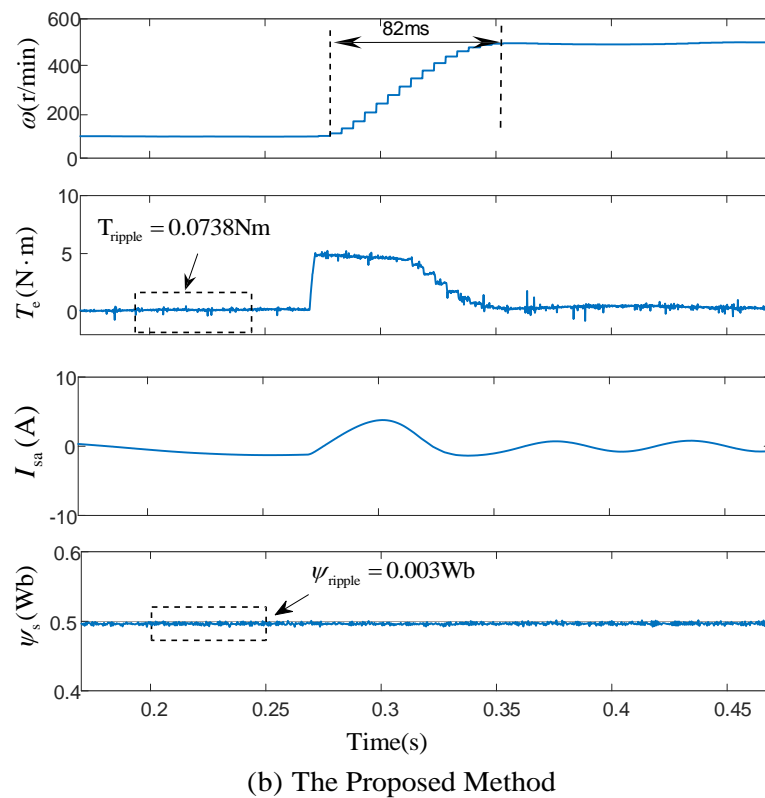
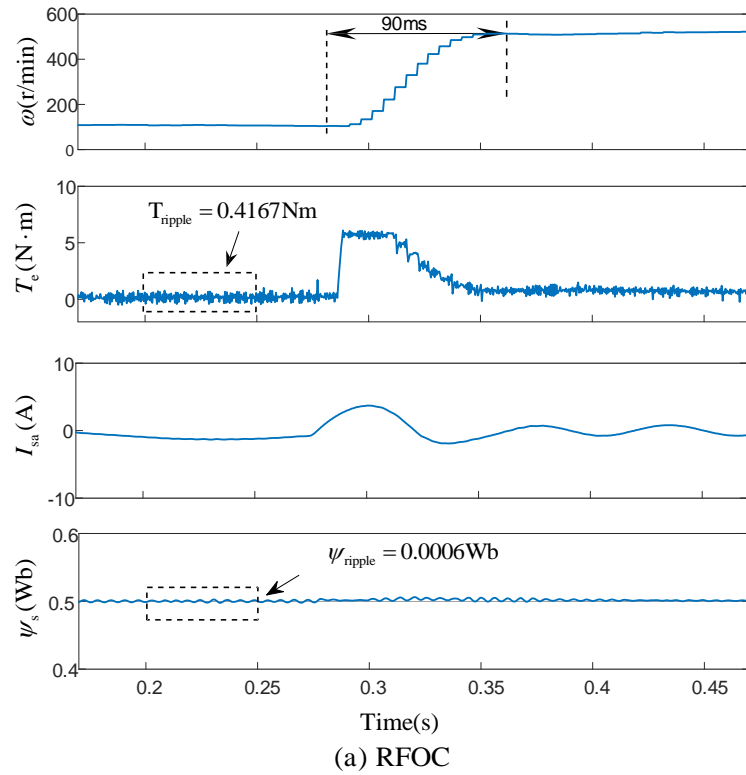


Figure 5. Cont.

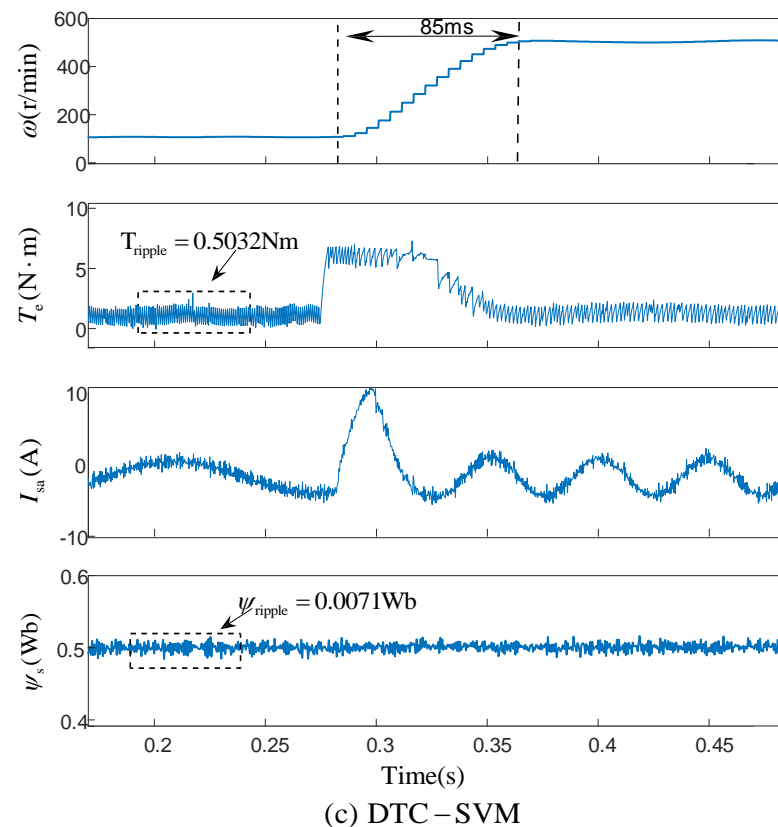


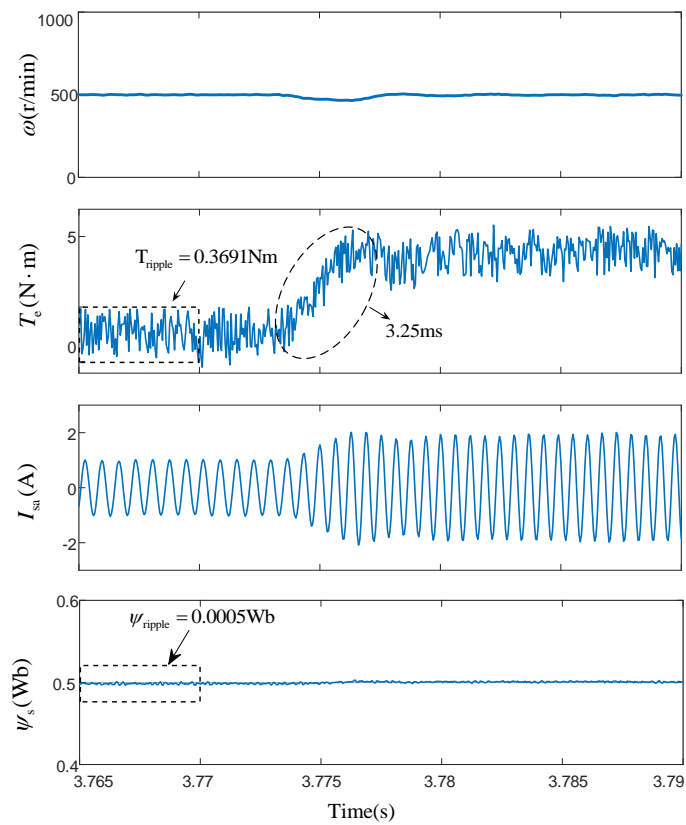
Figure 5. Speed response results: (a) RFOC; (b) proposed method; (c) DTC–SVM.

4.2. Step Torque Transient Characteristics

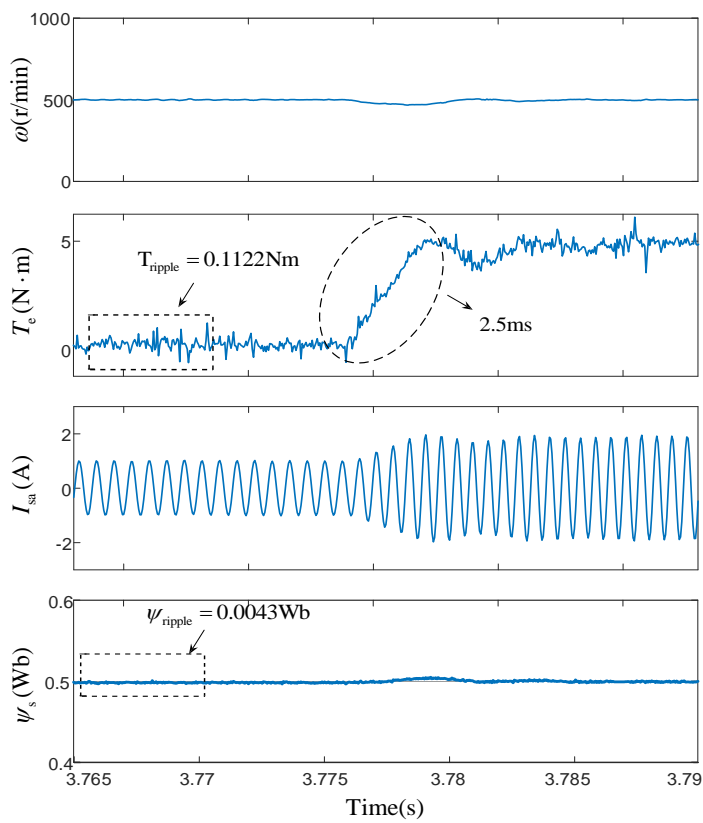
As shown in Figure 6, the transient torque step response characteristics of the three methods were tested. The motor was started without a load and then maintain at a speed of 500 rpm; then, the torque was increased by 5 Nm. The torque speed increase of RFOC was 1.538 Nm/ms, whereas for the proposed method, it was 2 Nm/ms and for the DTC 1.8115 Nm/ms. The torque response of the proposed method was 30% faster than that of RFOC and 10% faster than that of DTC–SVM.

RFOC controlled the current through current feedback, then it controlled the magnetic field, and finally, it controlled the motor movement. The proposed method directly used the dual torque signal as the feedback inner loop, without the current loop, which accelerated the torque response speed, as compared to RFOC.

The torque response of DTC–SVM was faster than that of RFOC because DTC used voltages to control the magnetic field. The torque response of the proposed method was better than that of DTC, because it directly takes dual torque as the control object, and the control model did not involve a magnetic field.



(a) RFOC



(b) The Proposed Method

Figure 6. Cont.

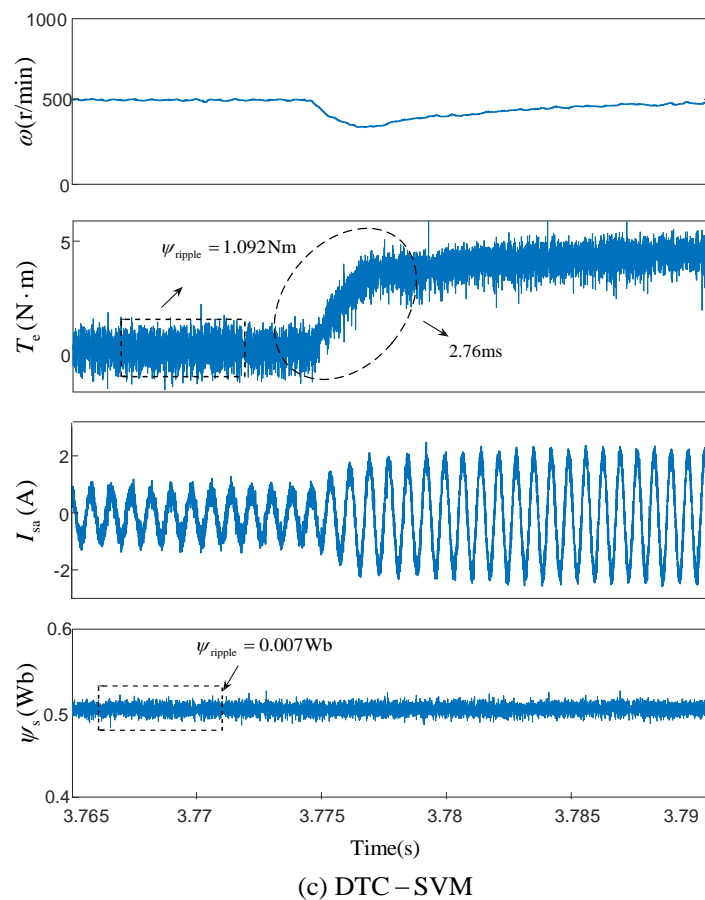
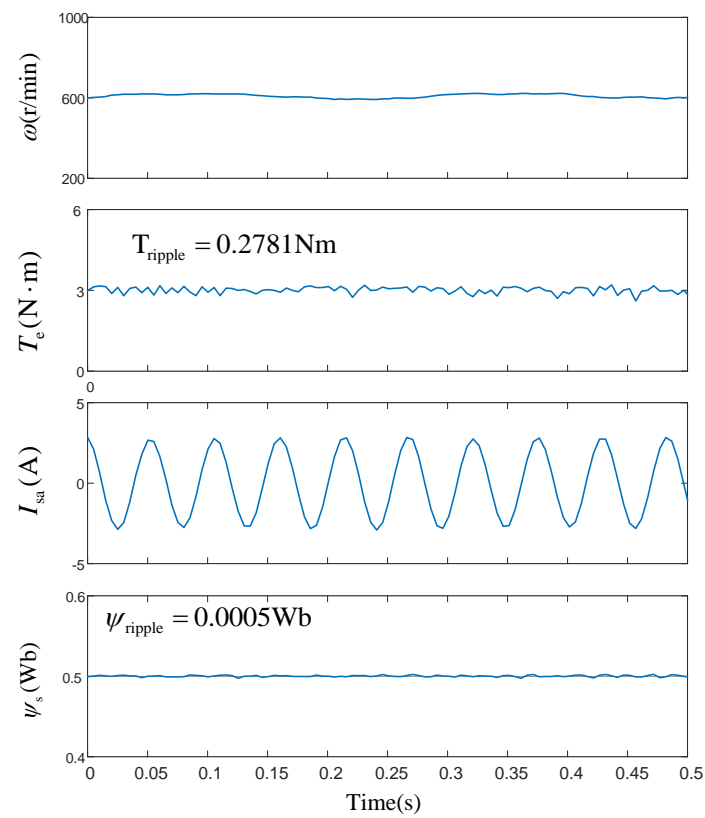


Figure 6. Torque Response Results: (a) RFOC; (b) proposed method; (c) DTC–SVM.

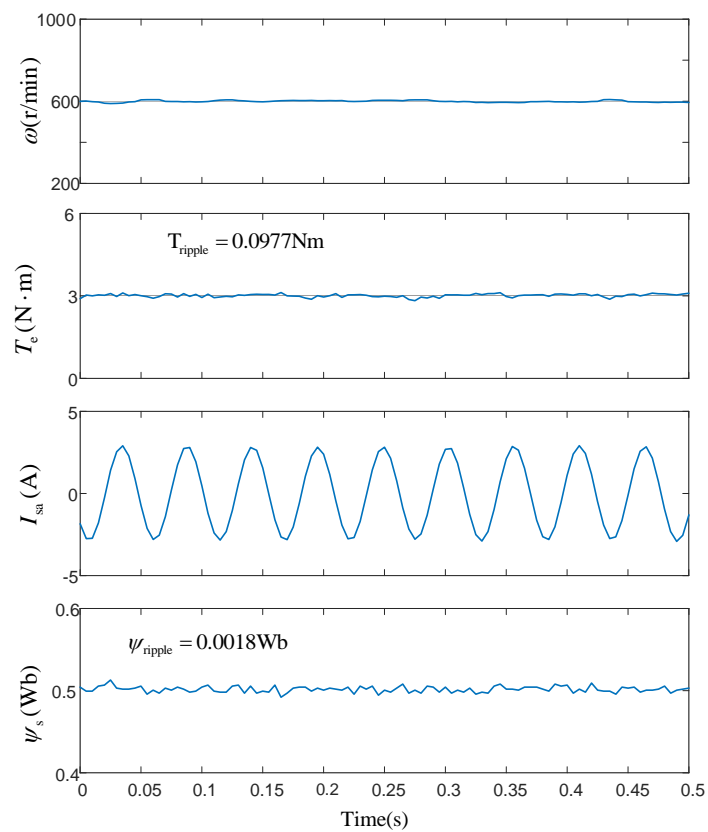
4.3. Steady-State Operations

Finally, the steady-state characteristics of the three methods shown in Figure 7 were tested at 600 r/min with 3 N · m load. Based on the calculation of Formula (55), the torque ripples of RFOC were 0.2781 N · m, the torque ripples of the proposed method were 0.0977 N · m, and the torque ripples of DTC–SVM were 0.5836 N · m. The torque ripples of the proposed method were 65% less than that of RFOC and 84% less than that of DTC–SVM. In addition, according to the experimental results, the stator flux ripples of the proposed method were 0.0043 N · m, and the stator flux ripples of DTC–SVM were 0.007 N · m, so the flux ripples of the proposed method were 39.6% lower than that of DTC–SVM. Therefore, the proposed method could effectively reduce torque and flux ripples.

The proposed method was based on the dual-torque model, which was naturally perpendicular in physical space, so it had natural decoupling ability, which made it ideal for designing decoupling controllers. Moreover, since perpendicular is natural and the perpendicular was invariable, no other conditions were needed, which made the decoupling ability of the dual-torque model stronger than that of RFOC.



(a) RFOC



(b) The Proposed Method

Figure 7. Cont.

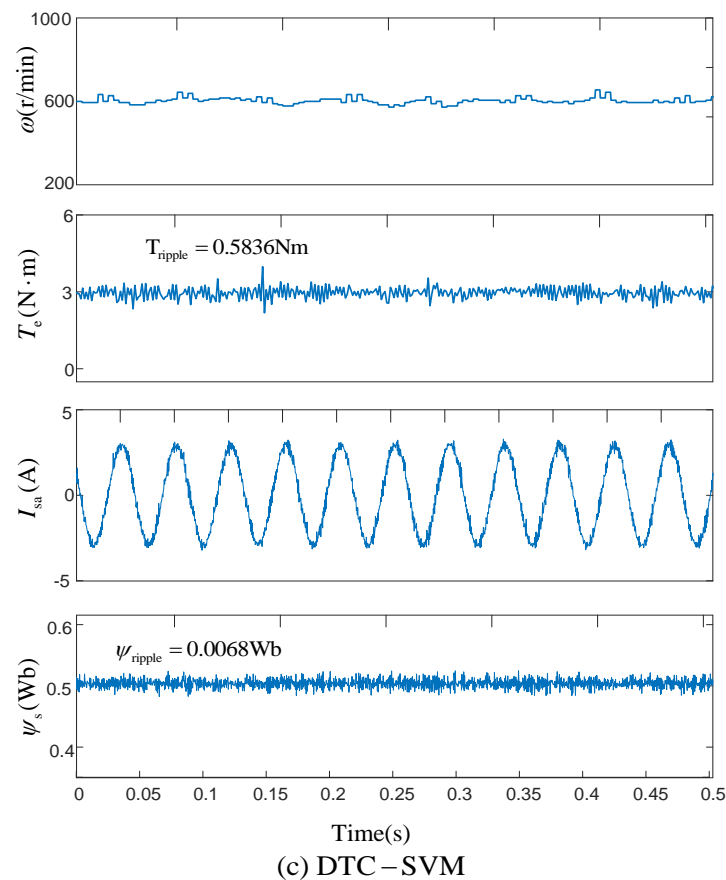


Figure 7. Steady operation results: (a) RFOC; (b) proposed method; (c) DTC–SVM.

5. Conclusions

In order to improve the transient and steady-state control performance of motors, this paper proposed a new control algorithm that includes a new IM model, a simplified linearization method, and a new control system structure. The research conclusions of this article are as follows:

- (1) The transient process of IM is actually the transient process of the rotating magnetic field. The proposed concepts of reactive torque and electromagnetic torque are an abstraction of the forces acting on the radial and tangential motions of the rotating magnetic field, respectively. These two variables accurately described the motor's rotating magnetic field transient. The reactive torque represented the amplitude of the rotating magnetic field, and the electromagnetic torque represented the rotating angular frequency of the magnetic field, rather than the phase.
- (2) The dual-torque model was a fourth-order model described by the reactive torque η_s , the electromagnetic torque τ_s , the amplitude ψ_s , and the rotational angular frequency ω . Using a dual-torque model instead of a conventional fifth-order model can greatly simplify the feedback linearization process and avoided zero-dynamic problems.
- (3) The proposed dual-torque model directly related the input instantaneous power to the torque dynamics. Therefore, this paper proposed dual-torque inner-loop feedback that improves the torque response speed.
- (4) This paper showed that the dual-torque model could be transformed into a singular perturbation model with the leakage inductance coefficient σ as the disturbance parameter. Therefore, this article proposed a control system based on time scale layering, which reduced the steady-state ripples.
- (5) The experimental results showed that the steady-state torque ripples of the proposed algorithm were reduced by 65%, as compared to RFOC, and by 84%, as compared

to DTC–SVM. In addition, the transient torque response speed was 30% faster than RFOC and 10% faster than DTC–SVM.

In order to further improve the engineering feasibility of the algorithm, the robustness of the proposed algorithm versus the parameter changes could be researched in the future.

Author Contributions: Conceptualization, X.C.; methodology, X.C.; software, X.C.; validation, X.C.; formal analysis, X.C.; investigation, X.C.; resources, X.C.; data curation, X.C.; writing—original draft preparation, X.C.; writing—review and editing, P.G.; visualization, X.C.; supervision, X.C.; project administration, X.C. All authors have read and agreed to the published version of the manuscript.

Funding: This research received no external funding.

Data Availability Statement: The data sources employed for analysis are presented in the text.

Conflicts of Interest: The authors declare no conflict of interest.

Appendix A

Table A1. Order of Magnitude for Common Time Constants of Induction Motors.

Symbol	Quantity	Order of Magnitude
τ_ω	Rotational speed time constant	1000 ms
τ_ψ	Magnetic flux time constant	100 ms
τ_σ	Torque time constant	1 ms

Table A2. Induction motor ratings and parameters.

Symbol	Quantity	Value
P_N	Rated shaft power	2.2 kW
U	Rated voltage	380 V
f	Rated frequency	50 Hz
ω	Rated speed	1422 r/min
n_p	Pole pairs	2
R_s	Stator resistance	3.4 Ω
R_r	Rotor resistance	2.444 Ω
L_s	Stator inductance	0.2724 H
L_r	Rotor inductance	0.2715 H
L_m	Mutual inductance	0.2631 H
J	Machine inertia	0.005 kg·m ²

References

- Liu, C.; Chau, K.T.; Lee, C.H.T.; Song, Z. A Critical Review of Advanced Electric Machines and Control Strategies for Electric Vehicles. *Proc. IEEE* **2021**, *109*, 1004–1028. [[CrossRef](#)]
- Yang, Z.; Shang, F.; Brown, I.P.; Krishnamurthy, M. Comparative Study of Interior Permanent Magnet, Induction, and Switched Reluctance Motor Drives for EV and HEV Applications. *IEEE Trans. Transp. Electrification* **2015**, *1*, 245–254. [[CrossRef](#)]
- Alsofyani, I.M.; Bak, Y.; Lee, K.-B. Fast Torque Control and Minimized Sector-Flux Droop for Constant Frequency Torque Controller Based DTC of Induction Machines. *IEEE Trans. Power Electron.* **2019**, *34*, 12141–12153. [[CrossRef](#)]
- Attaianesi, C.; Di Monaco, M.; Spina, I.; Tomasso, G. A Variational Approach to MTPA Control of Induction Motor for EVs Range Optimization. *IEEE Trans. Veh. Technol.* **2020**, *69*, 7014–7025. [[CrossRef](#)]
- Hinkkanen, M.; Awan, H.; Qu, Z.; Tuovinen, T.; Briz, F. Current Control for Synchronous Motor Drives: Direct Discrete-Time Pole-Placement Design. *IEEE Trans. Ind. Appl.* **2015**, *52*, 1530–1541. [[CrossRef](#)]
- Thike, R.; Pillay, P. Characterization of a Variable Flux Machine for Transportation Using a Vector-Controlled Drive. *IEEE Trans. Transp. Electrification* **2018**, *4*, 494–505. [[CrossRef](#)]
- Su, J.; Gao, R.; Husain, I. Model Predictive Control Based Field-Weakening Strategy for Traction EV Used Induction Motor. *IEEE Trans. Ind. Appl.* **2018**, *54*, 2295–2305. [[CrossRef](#)]
- Abosh, A.H.; Zhu, Z.Q.; Ren, Y. Reduction of Torque and Flux Ripples in Space Vector Modulation-Based Direct Torque Control of Asymmetric Permanent Magnet Synchronous Machine. *IEEE Trans. Power Electron.* **2017**, *32*, 2976–2986. [[CrossRef](#)]
- Wang, B.; Zhang, J.; Yu, Y.; Zhang, X.; Xu, D. Unified Complex Vector Field-Weakening Control for Induction Motor High-Speed Drives. *IEEE Trans. Power Electron.* **2021**, *36*, 7000–7011. [[CrossRef](#)]

10. Alsofyani, I.M.; Lee, K.-B. Enhanced Performance of Constant Frequency Torque Controller-Based Direct Torque Control of Induction Machines with Increased Torque-Loop Bandwidth. *IEEE Trans. Ind. Electron.* **2020**, *67*, 10168–10179. [[CrossRef](#)]
11. Masoumkhani, H.; Taheri, A. PI Regulator-Based Duty Cycle Control to Reduce Torque and Flux Ripples in DTC of Six-Phase Induction Motor. *IEEE J. Emerg. Sel. Top. Power Electron.* **2021**, *9*, 354–370. [[CrossRef](#)]
12. Lin, X.; Huang, W.; Jiang, W.; Zhao, Y.; Zhu, S. Deadbeat Direct Torque and Flux Control for Permanent Magnet Synchronous Motor Based on Stator Flux Oriented. *IEEE Trans. Power Electron.* **2020**, *35*, 5078–5092. [[CrossRef](#)]
13. Jing, B.; Dang, X.; Liu, Z.; Ji, J. Torque Ripple Suppression of Switched Reluctance Motor with Reference Torque Online Correction. *Machines* **2023**, *11*, 179. [[CrossRef](#)]
14. Forestieri, J.N.; Farasat, M.; Trzynadlowski, A.M. Indirect Real- and Reactive-Power Control of Induction Motor Drives. *IEEE J. Emerg. Sel. Top. Power Electron.* **2018**, *6*, 2109–2125. [[CrossRef](#)]
15. Kwak, B.; Um, J.-H.; Seok, J.-K. Direct Active and Reactive Power Control of Three-Phase Inverter for AC Motor Drives With Small DC-Link Capacitors Fed by Single-Phase Diode Rectifier. *IEEE Trans. Ind. Appl.* **2019**, *55*, 3842–3850. [[CrossRef](#)]
16. Liu, Y.; Vittal, V.; Undrill, J. Performance-Based Linearization Approach for Modeling Induction Motor Drive Loads in Dynamic Simulation. *IEEE Trans. Power Syst.* **2017**, *32*, 4636–4643. [[CrossRef](#)]
17. Morawiec, M.; Lewicki, A. Speed Observer Structure of Induction Machine Based on Sliding Super-Twisting and Backstepping Techniques. *IEEE Trans. Ind. Inform.* **2021**, *17*, 1122–1131. [[CrossRef](#)]
18. Ho, M.-T.; Tu, Y.-W.; Lin, H.-S. Controlling a ball and wheel system using full-state-feedback linearization [Focus on Education]. *IEEE Control Syst.* **2009**, *29*, 93–101. [[CrossRef](#)]
19. Accetta, A.; Cirrincione, M.; Pucci, M.; Sferlazza, A. Feedback Linearization Based Nonlinear Control of SynRM Drives Accounting for Self- and Cross-Saturation. *IEEE Trans. Ind. Appl.* **2022**, *58*, 3637–3651. [[CrossRef](#)]
20. Li, H.; Wang, Z.; Xu, Z.; Wang, X.; Hu, Y. Feedback Linearization Based Direct Torque Control for IPMSMs. *IEEE Trans. Power Electron.* **2021**, *36*, 3135–3148. [[CrossRef](#)]
21. Zhao, Y.; Yu, H.; Wang, S. Development of Optimized Cooperative Control Based on Feedback Linearization and Error Port-Controlled Hamiltonian for Permanent Magnet Synchronous Motor. *IEEE Access* **2021**, *9*, 141036–141047. [[CrossRef](#)]
22. Zhong, Z.; Wang, J. Looper-Tension Almost Disturbance Decoupling Control for Hot Strip Finishing Mill Based on Feedback Linearization. *IEEE Trans. Ind. Electron.* **2011**, *58*, 3668–3679. [[CrossRef](#)]
23. Choi, Y.-S.; Choi, H.H.; Jung, J.-W. Feedback Linearization Direct Torque Control With Reduced Torque and Flux Ripples for IPMSM Drives. *IEEE Trans. Power Electron.* **2016**, *31*, 3728–3737. [[CrossRef](#)]
24. Lascu, C.; Jafarzadeh, S.; Fadali, M.S.; Blaabjerg, F. Direct Torque Control With Feedback Linearization for Induction Motor Drives. *IEEE Trans. Power Electron.* **2017**, *32*, 2072–2080. [[CrossRef](#)]
25. Isidori, A. *Nonlinear Control System*, 2nd ed.; Springer: Berlin/Heidelberg, Germany, 1989; pp. 145–183.
26. Marino, R.; Peresada, S.; Valigi, P. Adaptive Input-Output Linearizing Control of Induction Motors. *IEEE Trans. Autom. Control* **1993**, *38*, 208–221. [[CrossRef](#)]

Disclaimer/Publisher’s Note: The statements, opinions and data contained in all publications are solely those of the individual author(s) and contributor(s) and not of MDPI and/or the editor(s). MDPI and/or the editor(s) disclaim responsibility for any injury to people or property resulting from any ideas, methods, instructions or products referred to in the content.